

MAGNETIC FIELDS IN EVOLVED STARS: IMAGING THE POLARIZED EMISSION OF HIGH-FREQUENCY SiO MASERS

W. H. T. VLEMMINGS¹, E. M. L. HUMPHREYS² & R. FRANCO-HERNÁNDEZ¹
Accepted for publication in ApJ

ABSTRACT

We present Submillimeter Array observations of high frequency SiO masers around the supergiant VX Sgr and the semi-regular variable star W Hya. The $J = 5 - 4$, $v = 1$ ²⁸SiO and $v = 0$ ²⁹SiO masers of VX Sgr are shown to be highly linearly polarized with a polarization from $\sim 5 - 60\%$. Assuming the continuum emission peaks at the stellar position, the masers are found within ~ 60 mas of the star, corresponding to ~ 100 AU at a distance of 1.57 kpc. The linear polarization vectors are consistent with a large scale magnetic field, with position and inclination angles similar to that of the dipole magnetic field inferred in the H₂O and OH maser regions at much larger distances from the star. We thus show for the first time that the magnetic field structure in a circumstellar envelope can remain stable from a few stellar radii out to ~ 1400 AU. This provides further evidence supporting the existence of large scale and dynamically important magnetic fields around evolved stars. Due to a lack of parallactic angle coverage, the linear polarization of masers around W Hya could not be determined. For both stars we observed the ²⁸SiO and ²⁹SiO isotopologues and find that they have a markedly different distribution and that they appear to avoid each other. Additionally, emission from the SO $5_5 - 4_4$ line was imaged for both sources. Around W Hya we find a clear offset between the red- and blue-shifted SO emission. This indicates that W Hya is likely host to a slow bipolar outflow or a rotating disk-like structure.

Subject headings: Masers, Polarization, Stars: Individual (VX Sgr, W Hya), Stars: Late-Type

1. INTRODUCTION

Many different SiO maser transitions have been observed around evolved stars of different classes (Kemball 2007, and references therein). High angular resolution observations of 43 and 86 GHz masers have shown that they occur within a few stellar radii from the photosphere, in the dynamical region between the pulsating star and the dust formation zone (e.g. Cotton et al. 2004; Greenhill et al. 1995; Chen et al. 2006). SiO masers are therefore excellent probes of the processes that drive stellar mass loss, and that define the outflows that give rise to potential asymmetries in the circumstellar envelope (CSE).

SiO maser emission from evolved stars has been detected from the $v = 0$ to $v = 4$, $J = 1 - 0$ up to at least the $J = 8 - 7$ transitions (e.g., Gray, Humphreys & Yates 1999; Pardo et al. 1998; Humphreys et al. 1997; Jewell et al. 1987). The conditions giving rise to emission are typically $n(\text{H}_2) = 10^{10 \pm 1} \text{ cm}^{-3}$ and $T_k \gtrsim 1500$ K, with the dominant pumping mechanism, radiative or collisional, a matter of debate (e.g. Herpin & Baudry 2000; Lockett & Elitzur 1992). However, it is agreed that line overlaps between the SiO main isotopologues (²⁸SiO, ²⁹SiO and ³⁰SiO) likely play a role in the pumping of e.g., the very highly excited $v = 4$ $J = 5 - 4$ maser line (~ 7000 K above ground state; Cernicharo et al. 1993). SiO maser $v = 1$ and 2, $J = 5 - 4$ emission is commonly found toward Mira variables for which the lower- J masers have already been detected. High-frequency SiO maser emission in Miras appears to be strongly tied to stellar pulsation, with the velocity of the emission a function of phase, and this phase dependence correlated with photon luminosity. Indeed, the $J = 7 - 6$ and $8 - 7$ lines are weak or absent from $\phi = 0.4$ to 0.7 , unlike the low- J masers (Gray et al. 1999). Humphreys (1999) finds that highly rotationally excited

SiO maser lines arise from a subset of the physical conditions leading to $J = 1 - 0$ emission, and are strongest in dense, warm post-shock gas.

Besides probing the dynamics and physical conditions in the CSEs, masers are also good probes of the magnetic field (e.g. Vlemmings 2007). Most of the information on the magnetic field around evolved stars comes from maser polarization observations. Ordered magnetic fields with a strength of order a mG have been detected in the OH maser regions at large distances from the star (e.g. Szymczak et al. 1998). Closer in, H₂O masers also indicate the presence of a dynamically important magnetic field, with typical values of a few hundred mG (e.g. Vlemmings et al. 2005). Finally, 43 and 86 GHz SiO maser observations reveal field strengths of several Gauss at only a few stellar radii from the star, assuming a standard Zeeman interpretation (Kemball & Diamond 1997; Herpin et al. 2006). The higher frequency SiO masers display a large fractional linear polarization (Shinnaga et al. 2004, hereafter S04), and this polarization is potentially a good probe of the circumstellar magnetic field morphology. However, as these masers likely exist in the regime where the Zeeman splitting is comparable to the rate of stimulated maser emission, the interpretation of their polarization is not straightforward (Nedoluha & Watson 1994).

Here we present the polarization and distribution of the $v = 1$ and 2 $J = 5 - 4$ ²⁸SiO and $v = 0$, $J = 5 - 4$ ²⁹SiO masers around the supergiant VX Sgr and the semi-regular variable star W Hya observed with the Submillimeter Array (SMA; Ho et al. 2004). In the remainder of the paper we will forgo most mentions of the rotational quantum numbers $J = 5 - 4$ and only give the vibrational quantum number $v = 0, 1$ or 2. In addition to the maser observations, we present observations of the SO $5_5 - 4_4$ line that was detected for both stars.

VX Sgr is a red supergiant star, located at a distance of 1.57 ± 0.27 kpc (Chen et al. 2007). It has an optical

¹ Argelander-Institut für Astronomie, University of Bonn, Auf dem Hügel 71, D-53121 Bonn, Germany

² ESO, Karl-Schwarzschild-Str. 2, D-85748 Garching, Germany

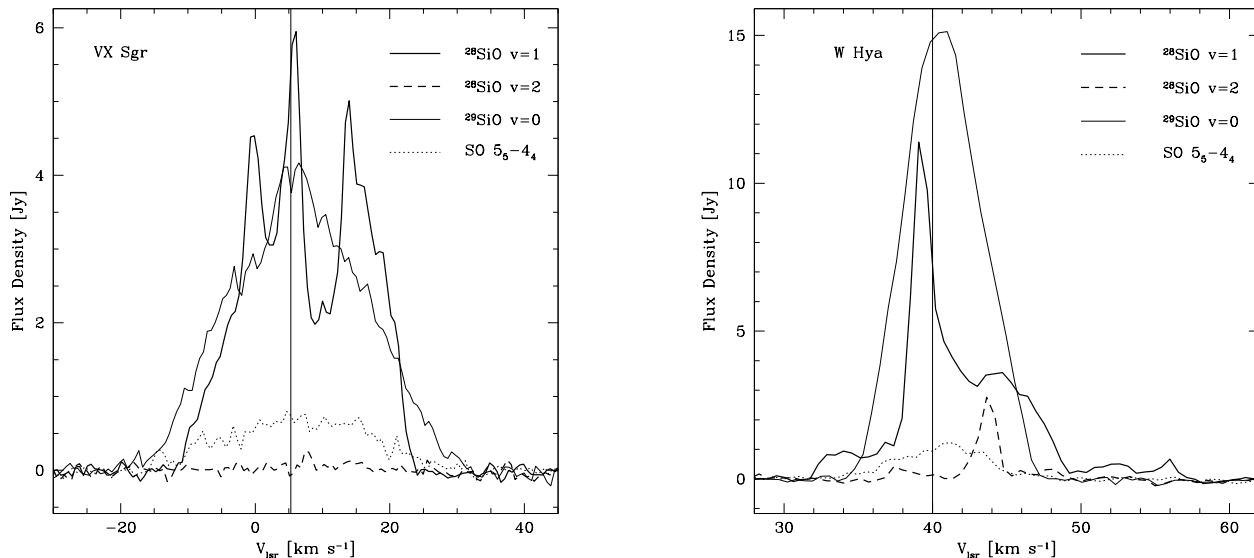


FIG. 1.— SMA spectra of VX Sgr (left) and W Hya (right) for the $^{28}\text{SiO } v=1, J=5-4$ masers at 215.6 GHz (thick solid line), the $^{28}\text{SiO } v=2, J=5-4$ masers at 214.1 GHz (thick dashed line), the $^{29}\text{SiO } v=0, J=5-4$ masers at 214.4 GHz (thin solid line) as well as the SO 5_5-4_4 line at 215.2 GHz (thin dotted line). The vertical lines denote the stellar velocity.

variability period of 732 days which suggests, assuming the Mira period-luminosity relation, it has a mass of $\sim 10 M_{\odot}$. Its envelope hosts a number of maser species, from which the stellar velocity is estimated to be $V_{\text{lsr}} = 5.3 \text{ km s}^{-1}$ (Chapman & Cohen 1986).

W Hya, at a distance of 98 pc (Vlemmings et al. 2003), is typically classified as a semi-regular variable star as its period is observed to vary between $\sim 350-400$ days. However, it is also often considered a Mira variable due to the regular shape and the large amplitude of its light curve (e.g. Gomez Balboa & Lepine 1986). The envelope of W Hya harbors many different maser species, and its OH maser spectrum indicates a stellar velocity of $V_{\text{lsr}} = 40 \text{ km s}^{-1}$ (Szymczak et al. 1998).

2. OBSERVATIONS

The SiO masers of VX Sgr and W Hya were observed on UTC 2008 July 20 with the SMA in extended configuration. The resulting beam size was $\sim 1.5 \times 1.0$ arcseconds. The observations were centered at 214.8 GHz ($\lambda = 1.4 \text{ mm}$) to allow simultaneous observation of both the $v=1$ and $v=2$ ^{28}SiO maser lines at 215.5959 and 214.0885 GHz respectively in one 2 GHz band. This additionally covered the frequencies of the $^{29}\text{SiO } v=0$ maser and the SO 5_5-4_4 line. The frequency resolution was 400 kHz, corresponding to $\sim 0.56 \text{ km s}^{-1}$. The 2 GHz bandwidth, excluding the channels with line emission, was used to observe the dust continuum. For the relative amplitude and phase calibration of VX Sgr we used NRAO530 ($\sim 12.4^\circ$ away; 2.45 Jy) and for W Hya we used 1337-129 ($\sim 15.8^\circ$ away; 2.4 Jy). For the absolute amplitude calibration we used 3C454.3 with a flux density of 22.63 Jy. In both cases we used the brightest $v=1$, ^{28}SiO maser to self-calibrate the data. We estimate the absolute positions to be accurate to ~ 0.2 arcseconds, while the relative positional accuracy of the different maser species and the dust should be good to better than $\sim 15 \text{ mas}$. The data were

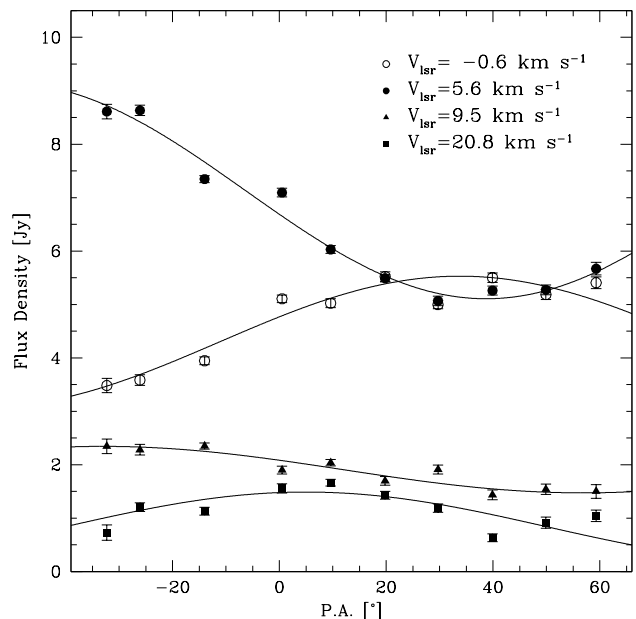


FIG. 2.— The feed position angle (P.A.) vs. the apparent flux density for four of the $^{28}\text{SiO } v=1, J=5-4$ masers around VX Sgr. The error bars denote the uncertainties on the flux density as derived by the *jmfit* Gaussian fitting procedure and do not contain potential systematic effects due to time variable errors in the gain calibration.

initially calibrated using the MIR IDL package, continuum subtraction and averaging was performed in MIRIAD, and the imaging and phase self-calibration was performed in AIPS. The channel rms noise is ~ 0.05 Jy beam $^{-1}$.

After imaging and self-calibration we used the AIPS image-plane component fitting task *jmfit* to determine the position of the maser emission in each individual velocity channel. When emission is detected at $> 10\sigma$, we define the fitted position in each channel as a maser spot following the definition of Chen et al. (2006). A maser feature is then a group of maser spots that occurs within a small spatial and spectral region. Very Long Baseline Interferometry (VLBI) SiO maser observations at high frequency resolution indicate that there are typically several tens of such features with line-widths of order 1 km s $^{-1}$ and a typical size of ~ 1 AU (e.g. Chen & Shen 2008). Both the spectral as well as the spatial resolution of our observations are insufficient to identify individual maser features. The maser spots defined here thus denote the flux weighted average position of features that contribute flux in the individual velocity channels. As the beam size (half-power beam width, HPBW) of our observations is $\sim 1.5 \times 1.0$ arcseconds, the formal position errors on the masers depend on the signal-to-noise ratio (SNR) at which the maser spots were detected through $\Delta(\delta, \alpha) = \text{HPBW}/(2 \times \text{SNR})$.

As was performed by S04, we measured the linear polarization by using earth rotation polarimetry, the diurnal rotation of the sky over the SMA. As the SMA antennas have alt-azimuth mounts and fixed linearly-polarized feeds at the Nasmyth focus, the position angle (P.A.) of the feeds on the sky rotates during the observations according to Equation 1 of S04:

$$\text{P.A.} [^\circ] = 45^\circ - a - \sin \frac{\cos(\phi_{\text{lat}}) \sin(h)}{\cos(a)}. \quad (1)$$

Here a and h are the elevation and hour angle of the source respectively, and ϕ_{lat} is the latitude of the SMA ($\sim 19^\circ 49' 27''$). For VX Sgr, h ranged from -2.3 to 2.8 hr and the P.A. varied from -35° to 60° . For W Hya, a delayed start of the observations resulted in an hour angle range of 0.6 to 3.4 hr and thus a smaller P.A. coverage from 15° to 75° .

3. ANALYSIS AND RESULTS

3.1. SiO Maser Spectra

The spectra for the SiO maser transitions as well as the SO line are shown in Fig. 1. Around VX Sgr, no significant emission was detected for the ^{28}SiO $v = 2$ transition. The $v = 1$ spectral profile has significantly changed compared with the detection in 1986 by Jewell et al. (1987) and the peak flux density decreased from ~ 15 to ~ 6 Jy. The ^{29}SiO emission is weaker, with a peak flux density of ~ 4 Jy and extends to slightly broader velocities with respect to the star. It also shows fewer individual features in the spectrum. Both lines peak close to the $V_{\text{lsr}} = 5.3$ km s $^{-1}$ stellar velocity.

The SiO maser emission of W Hya is stronger than that of VX Sgr in all the three lines observed. Although the peak flux density has decreased by a factor of 5, the ^{28}SiO $v = 1$ spectrum is remarkably similar to that observed by Jewell et al. (1987) over two decades earlier. It does not, however, resemble the spectrum obtained in

1995 (Humphreys et al. 1997). The shape of the ^{28}SiO $v = 2$ spectrum is significantly different from that of the $v = 1$ transition. Where the $v = 1$ line peaks around $V_{\text{lsr}} = 39$ km s $^{-1}$ with a flux density of ~ 11 Jy, the $v = 2$ maser is weaker (~ 3 Jy) and peaks at ~ 44 km s $^{-1}$. As was the case for VX Sgr, the ^{29}SiO maser spectrum has less structure than that of the ^{28}SiO masers, while it peaks close to the stellar velocity of $V_{\text{lsr}} = 40$ km s $^{-1}$. At 15 Jy, it is stronger than the ^{28}SiO lines.

3.2. Linear Polarization Analysis

Because of the rotation of the polarized feeds on the sky as described in § 2, the brightness S of a linearly polarized source changes as a function of feed position angle according to the equation

$$S = S_0 + S_p \cos[2(\text{P.A.} - \chi)]. \quad (2)$$

Here S_0 is the average and S_p the polarized brightness, and χ the electric-vector position angle (EVPA). The fractional linear polarization $P_l = S_p/S_0$. An example for four of VX Sgr maser spots is shown in Fig. 2.

For a sufficient range of P.A. it is thus possible to determine the EVPA and fractional polarization. We performed a least squares fit to all channels with significant ($> 10\sigma$) maser emission, having split the data in single 20 min blocks. The flux density and associated uncertainties of the individual observing blocks were determined using the AIPS task *jmfit*. Assuming a constant dust continuum flux density during the observations, we determined an initial gain factor for each of the time steps. The gain corrections derived from the dust were $\lesssim 6\%$, indicating that the dust was not polarized at a level higher than $\sim 6\%$. This, as well as the non-detection of polarization in the SO line, indicates that the observed SiO maser polarization is not an artifact of our self-calibration and further reduction process. Still, as using the dust for gain calibration could in principle introduce a systematic bias due to possible dust polarization at a level of a few percent, we also adopted the method described by S04 in an iterative minimization routine. This yielded final gain corrections for the individual time intervals of $2 - 9\%$. Still, remaining time variable uncertainties in the flux calibration will due to, for example, variable phase coherence add non-Gaussian errors to the flux density determinations. The influence of remaining systematic errors on the polarization fitting can be estimated using the bootstrap technique (e.g. Efron & Tibshirani 1991). This technique allows determination of the fitted values and their associated uncertainties without relying on Gaussian statistics and has previously been applied to assess image fidelity in radio interferometric polarimetry (Kemball & Martinsek 2005; Kembal et al. 2010). The bootstrap technique consists of the following; we treat the N data points S_i for each 20-min observing interval as a set of independent estimates for the flux density. We then generate data samples of size N generated from the original set with replacement, discarding samples with fewer than four independent measurements. We generate 100,000 of such data samples for which the least-squares fitting routine will determine their best fitting S_0 , S_p and χ . From the distribution of these sample we then determine the most probable value for each of the parameters as well as their most compact 68% confidence interval.

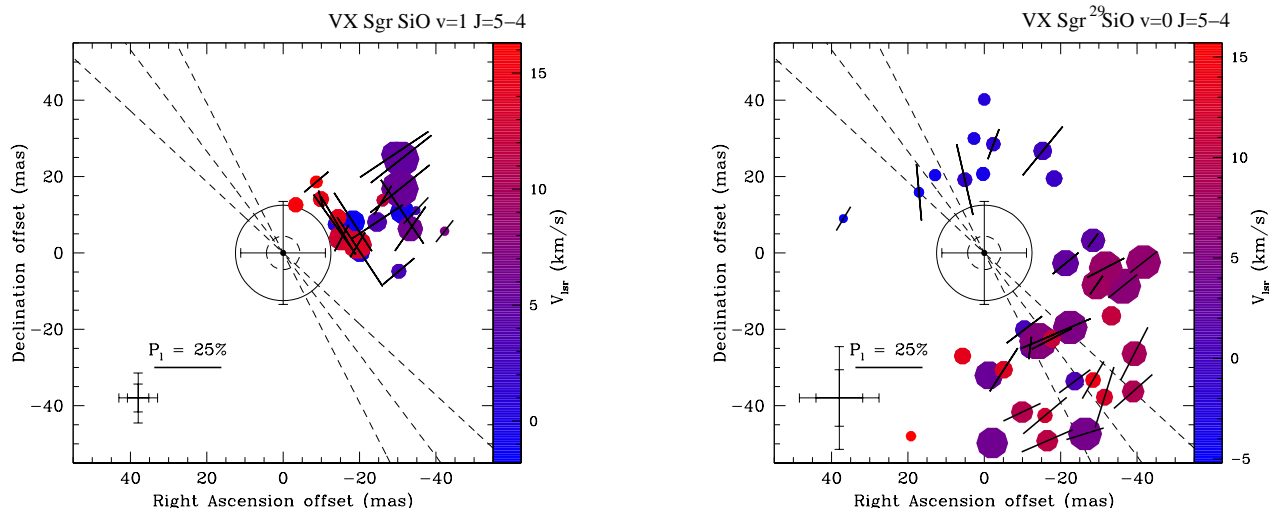


FIG. 3.— Positions and polarization of the $v = 1, J = 5 - 4$ ^{28}SiO (left) and $v = 0, J = 5 - 4$ ^{29}SiO masers (right) around VX Sgr. The masers spots are plotted with respect to peak of the dust emission ($\alpha_{J2000} = 18^h08^m04^s.068 \pm 0.014$ and $\delta_{J2000} = -22^\circ13'28''.416 \pm 0.200$). The uncertainty in the dust position relative to the masers is indicated by the error bars in the center. Also note the difference in velocity scale between the two transitions. The symbols are linearly scaled according to brightness (^{28}SiO : 3.8–6.9 Jy beam $^{-1}$; ^{29}SiO : 2.3–4.2 Jy beam $^{-1}$). For ^{28}SiO we only present the masers that were detected with a $\text{SNR} > 50$. For the weaker ^{29}SiO we plot the masers detected at $\text{SNR} > 30$. The minimum and maximum positional errors for the plotted maser spots are indicated by the error bars in the bottom left. The black vectors are the observed polarization vectors scaled linearly according to polarization fraction. The long dashed inner circle indicates the star with a radius of ~ 4.35 mas (Monnier et al. 2004) and the solid circle indicates the location of the 43 GHz SiO masers (Chen et al. 2006). The dashed lines indicate the position angle and its uncertainty of the inferred orientation of the dipole magnetic field of VX Sgr observed using H_2O and OH masers (Vlemmings et al. 2005; Szymczak et al. 2001).

3.2.1. VX Sgr

The polarization fractions and angles for the SiO masers of VX Sgr are given in the online Table.1 and shown in Fig. 3. The uncertainties are derived using the aforementioned bootstrap method. We find that the average polarization fraction of the ^{28}SiO $v = 1$ masers $\langle P_l \rangle = 26 \pm 16\%$ with the highest value reaching almost 80%. The maser EVPA χ has, as seen in Fig 4, a bimodal distribution, with peaks at $\langle \chi \rangle = -44 \pm 13^\circ$ and $\langle \chi \rangle = 29 \pm 11^\circ$. The ^{29}SiO masers have a slightly lower average polarization $\langle P_l \rangle = 22 \pm 12\%$ with the highest fractional polarization measured being 60%. The maser EVPA distribution is somewhat wider and not bimodal, and has $\langle \chi \rangle = -47 \pm 22^\circ$. No significant polarization was measured for the SO emission.

3.2.2. W Hya

The P.A. range for W Hya was too small to perform independent fits to both EVPA and polarization fraction. We thus performed a number of fits with fixed P_l or χ . However, these did not allow for strong conclusions beyond that the mean fractional linear polarization is consistent with those found for the masers for VX Sgr.

3.3. Maser Distribution

The maser distributions of VX Sgr and W Hya are shown in Figs. 3 and 5. The formal position errors on the masers are large and depend on the signal-to-noise ratio (SNR). We therefore only present those masers detected with a high SNR, whose positions are determined with better than ~ 10 mas accuracy. The distributions of the ^{28}SiO and ^{29}SiO masers around VX Sgr are presented individually with respect to the peak of the dust emission, which was determined with an accuracy of ~ 14 mas

(corresponding to ~ 24 AU).

Some evidence for asymmetry in the dust envelope of VX Sgr has been seen using infrared interferometry (Monnier et al. 2004), and also the dust emission peak of the supergiant VY CMa appears offset from the SiO maser emission (Muller et al. 2007). However, if the dust peak of VX Sgr denote the stellar position, the ^{28}SiO maser distribution is quite asymmetric. The ^{29}SiO maser spots however, do appear to occur around the dust peak. For W Hya no clear offset between the dust and the masers was seen, and the positions for all three maser transitions are presented together with respect to the peak of the dust emission. Still, because of possible asymmetry in the dust emission this is not necessarily the stellar position.

3.4. SO Emission

Emission from the SO $5_5 - 4_4$ transition at 215.2 GHz was detected for both VX Sgr and W Hya and is shown in Fig. 1. Although more typically observed at higher and lower frequency transitions, sulfur bearing species are frequently found in the envelopes of O-rich stars (e.g. Omont et al. 1993). Sulfur is very reactive with OH and will form SO. The SO emission of both VX Sgr and W Hya covers only a small velocity range around the stellar velocity, a range comparable to that of the SiO masers. In both stars the emission peaks near the stellar velocities with a flux density of ~ 1 Jy. For W Hya, we find that, as indicated in Fig. 7, the peak of the integrated red-shifted emission between $40 - 47$ km s $^{-1}$ is offset from that of the blue-shifted emission between $33 - 47$ km s $^{-1}$. The separation between the emission peaks is 0.29 ± 0.04 arcseconds, which at the distance of W Hya corresponds to ~ 28 AU on the sky. The offset is almost exactly in the North-South direction, with a position angle of $3^\circ \pm 10^\circ$.

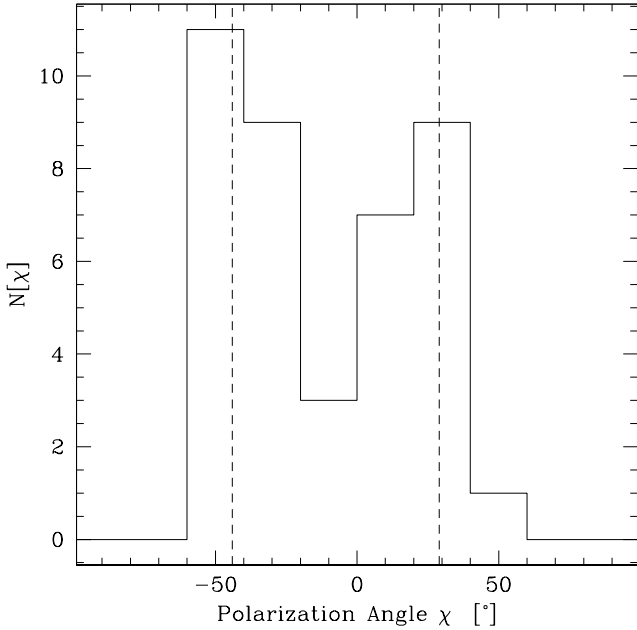


FIG. 4.— The distribution of the electric-vector position angles (χ) for the $v = 1, J = 5 - 4$ ^{28}SiO masers of VX Sgr. The dashed lines indicate the error weighted average peaks of the bimodal distribution of χ . The histogram was constructed using all detected maser spots indicated in Table.1.

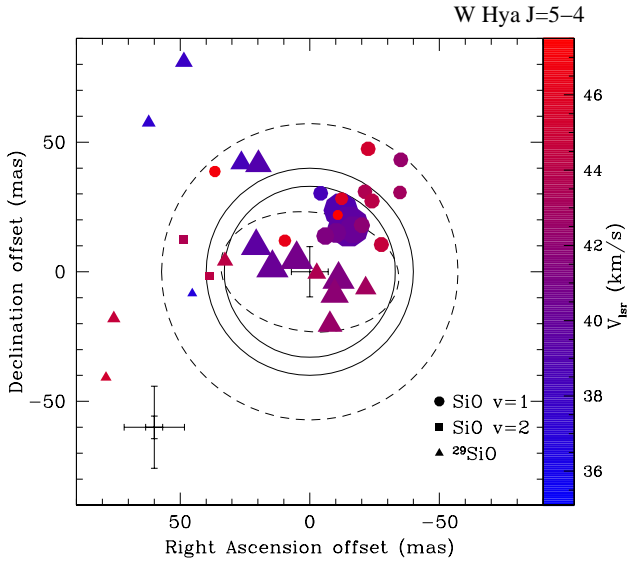


FIG. 5.— Positions of the $J = 5 - 4$ transitions of ^{29}SiO $v = 0$ and ^{28}SiO $v = 1,2$ around W Hya. Positions of the masers are with respect to the peak of the dust emission ($\alpha_{\text{J2000}} = 13^{\text{h}}49^{\text{m}}01^{\text{s}}.953 \pm 0.015$ and $\delta_{\text{J2000}} = -28^{\circ}22'06''.208 \pm 0.200$) for spots with a $\text{SNR} > 20$. The dust position is given in the center with positional uncertainties. The symbols are scaled linearly according to brightness, ranging from 2.2–11.1 Jy beam^{-1} . The minimum and maximum error bars of the plotted SiO maser spots are shown in the bottom right corner. The outer, dashed, circle indicates the inner dust shell as determined from models by Wishnow et al. (2010). The solid lines indicate the radius of the 43 GHz SiO maser observations at two epochs (Cotton et al. 2004, 2008). The dashed ellipse is the elongated radio-photosphere as determined by Reid & Menten (2007).

The SO emission of VX Sgr does not show a significant velocity separation and peaks at the same position as the dust as shown in Fig. 6.

3.5. Dust Continuum

The $\lambda = 1.4$ mm continuum emission toward both W Hya (Fig.7) and VX Sgr is unresolved. The integrated flux density of the W Hya emission is $S_{\nu} = 213 \pm 3$ mJy, a value comparable with previous measurements of 270 ± 15 mJy (SMA 1.1 mm; Muller et al. 2008), 280 ± 17 mJy (SIMBA 1.2 mm; Dehaes et al. 2007), and 280 ± 30 mJy (JCMT 1.1 mm; van der Veen et al. 1995), taking into account a lower stellar contribution to the flux at longer wavelength. In the case of VX Sgr, the total flux density $S_{\nu} = 95 \pm 2$ mJy. To our knowledge no previous millimeter dust measurements of VX Sgr are available for comparison.

4. DISCUSSION

4.1. The Location of the SiO Maser Transitions

The maser distributions shown in Figs. 3 and 5 do not show the clear circular morphology often seen in the 43 and 86 GHz SiO masers (e.g. Cotton et al. 2004; Soria-Ruiz et al. 2004). However, with the angular resolution provided by the SMA we cannot reach the sub-mas positional accuracy obtained with very long baseline interferometry for the lower frequency transitions. The ^{28}SiO maser spots of VX Sgr are offset from the peak of the dust emission by $\sim 28 \pm 14$ mas towards the North-West. However, the ^{29}SiO masers do show a hint of a circular distribution with an inner radius of ~ 18 mas, slightly more than the ~ 12 mas observed for the 43 GHz masers (Chen et al. 2006). The situation for W Hya is less clear, although for this source 43 GHz masers also display only an incomplete ring morphology (e.g. Cotton et al. 2008). Our observations do let us conclude that specifically the strongest of the ^{28}SiO and ^{29}SiO masers avoid each other,

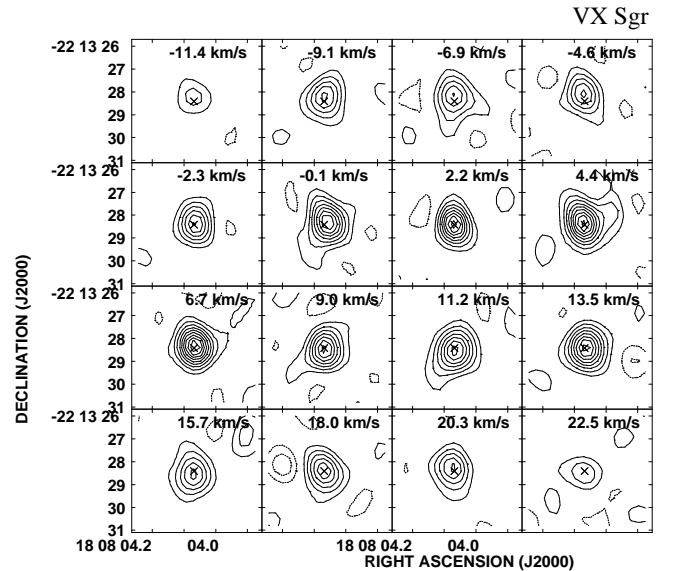


FIG. 6.— Contour plots of the SO $5_5 - 4_4$ emission around VX Sgr. The contours are drawn at 10% levels of the peak brightness ($795 \text{ mJy beam}^{-1}$). The cross denotes the peak position of the dust emission.

something that was also found for the 43 GHz ^{28}SiO and ^{29}SiO masers of IRC+10011 by Soria-Ruiz et al. (2005).

4.2. Linear Polarization

Masers can become linearly polarized under the influence of a magnetic field (Goldreich et al. 1973). Here we measured the linear polarization of the $J = 5 - 4$ SiO masers of VX Sgr to be up to $\sim 80\%$. This is consistent with the linear polarization fractions measured for the $v = 1, J = 5 - 4$ ^{28}SiO masers of VY CMa in S04. For the $J = 1 - 0$ SiO maser transitions, such polarization fractions can be reached due to interaction with a magnetic field of a few Gauss (e.g. Western & Watson 1984). However, for the higher J transitions, fractional linear polarization arising solely from interaction of a saturated maser with a magnetic field is expected to be much lower. Already for the $J = 2 - 1$ SiO maser transition, similar polarization fractions would need magnetic field strengths of > 10 G (Western & Watson 1984) and for $J = 5 - 4$ transitions this will be even higher. However, in the presence of anisotropic pumping, the linear polarization fraction can actually increase with the angular momentum of the involved state (Nedoluha & Watson 1994).

The high linear polarization is therefore largely due to anisotropic pumping of the maser. We now need to assess if the EVPA can still be used to derive the magnetic field morphology. As described in for example Nedoluha & Watson (1990) this depends on the ratios between the maser decay rate Γ , the maser stimulated emission rate R and the Zeeman frequency shift $g\Omega$. Assuming a typical magnetic field of 3.5 G (Herpin et al. 2006), the Zeeman frequency shift of the $J = 5 - 4$ SiO masers is $\sim 800 \text{ s}^{-1}$. The maser decay rate $\Gamma \sim 5 \text{ s}^{-1}$. The rate for

stimulated emission of the $J = 5 - 4$ SiO masers is given by $R \approx 4 \times 10^{-6} T_b \Delta\Omega$ (S04), where T_b is the maser brightness temperature and $\Delta\Omega$ its beaming angle. Assuming a maser spot size of ~ 0.4 AU similar to that of the VX Sgr 43 GHz SiO masers (Greenhill et al. 1995), the brightest masers in our observations have $T_b \sim 2 \times 10^9$ K and the weakest ones have a T_b almost two orders of magnitude less. Taking $\Delta\Omega \sim 10^{-2}$ sr (e.g. Reid & Moran 1988), this yields $R \sim 80$. Therefore $g\Omega > R, \Gamma$. For these values, the results from Nedoluha & Watson (1990) indicate that the linear polarization still traces the magnetic field direction, either parallel or perpendicular, even in the presence of anisotropic pumping. Specifically, the polarization vectors are parallel to the magnetic field if the angle between the field and the line-of-sight $\theta < \theta_{\text{crit}} \approx 55^\circ$ and perpendicular if $\theta > \theta_{\text{crit}}$, where θ_{crit} is the “van Vleck angle” (Goldreich et al. 1973).

4.3. The Shape of the Magnetic Field around VX Sgr

Observations of 1612 MHz OH maser polarization suggest that, in the OH maser region at ~ 1400 AU from VX Sgr, the magnetic field has a dipole shape with a position angle $\Theta = 210^\circ \pm 20$ and an inclination angle i between $20 - 30^\circ$ from the plane of the sky (Szymczak & Cohen 1997; Szymczak et al. 2001). A similar dipole configuration, with $\Theta = 220^\circ \pm 10$ and $i = 40^\circ \pm 5$ was found from H_2O polarization observations between $\sim 100 - 300$ AU from the star (Vlemmings et al. 2005).

We have now been able to probe the magnetic field structure at only $\sim 20 - 100$ AU from the star using SiO maser polarization observations. As seen in Fig.3, the masers indicate a large scale structure in the field with a preferred axis at $\sim 30^\circ$ or $\sim -45^\circ$, which, within the quoted uncertainties, is consistent with a 90° change of EVPA direction. Such a 90° flip has previously also been observed in the 43 GHz SiO masers, and is attributed to a change of the angle between the magnetic field and the line-of-sight θ through θ_{crit} (Kemball & Diamond 1997). This is consistent with a magnetic field with an inclination axis close to θ_{crit} , as the curvature of the magnetic field near the star would, close to the plane of the sky where most SiO masers are tangentially amplified, produce masers with θ both somewhat larger and smaller than θ_{crit} . Our SiO maser observations therefore suggest that the magnetic field close to the star has a morphology with an inclination axis $i \sim 90 - \theta_{\text{crit}} = 35^\circ$ and a position angle $\Theta \sim 135^\circ \pm 20$ or $\Theta \sim 210^\circ \pm 20$. These values are consistent with the likely dipole shaped field further out in the envelope, although a full 3-dimensional reconstruction of the field in the SiO maser region is complicated by the unknown location of the masers along the line of sight. Still, the SiO masers offer further strong evidence for a large-scale, most probably dipole-shaped, magnetic field around VX Sgr and, considering the other maser observations, a position angle of $\sim 210^\circ$ is most likely. Combining information from all three maser species at $20 - 1400$ AU distance from VX Sgr, we conclude that VX Sgr likely has a dipole magnetic field with $\Theta = 217^\circ \pm 7$ and $i = 37^\circ \pm 9$.

Having confirmed the existence of a similar large scale magnetic field from the SiO maser region out to the OH maser regions, we can extrapolate the fields measured on the OH and H_2O masers back to the SiO maser region at ~ 50 AU (Vlemmings et al. 2005). As, for a dipole magnetic

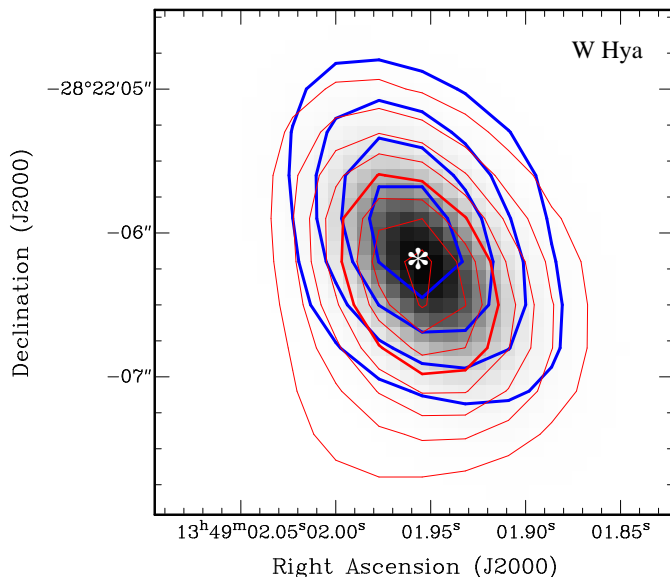


FIG. 7.— Contours of the integrated red-shifted ($V_{\text{lsr}} > 40 \text{ km s}^{-1}$; thin red) and blue-shifted ($V_{\text{lsr}} < 40 \text{ km s}^{-1}$; thick blue) SO $5_5 - 4_4$ emission around W Hya over-plotted on the dust emission (greyscale). Contours are drawn at intervals of 0.1 Jy beam^{-1} , starting at $0.05 \text{ Jy beam}^{-1}$ (4σ). The star denotes the peak position of the dust emission.

field, $B \propto R^{-3}$ and as the OH and H₂O maser distances from the star are only roughly known, the uncertainty on this extrapolation is large. Still, we find the field in the SiO maser region to be in the range of $B \sim 25 - 100$ G. While larger than the typical field found by Herpin et al. (2006), this is comparable to the $B = 87$ G field measured in the SiO region of VX Sgr by Barvainis et al. (1987).

4.4. The SO Envelope of W Hya

The detection of spatially offset red- and blue-shifted SO emission around W Hya reveals an asymmetry in the CSE. Previous high angular resolution SO observations indicate that the SO emission can be enhanced in collimated outflows and/or equatorial structures (e.g. Dinh-V.-Trung et al. 2009; Sánchez Contreras et al. 2000). This implies that W Hya harbors either a slow bipolar outflow or a rotating and possibly expanding equatorial disk. The position angle of the SO structure, measured between the peaks of the red- and blue-shifted SO emission, is $3^\circ \pm 10$, nearly perpendicular to the strongly elliptical radio-photophere measured by Reid & Menten (2007) to have a position angle of $83^\circ \pm 18$ and a size of 69×46 mas. Additionally, the red- and blue-shifted separation in SO is similar, both in scale, velocity and in position angle, to that observed in the OH maser region (Szymczak et al. 1998). From this it was inferred that the OH masers originated in a weak bipolar outflow or a tilted circumstellar disk. Our observations of the SO emission thus further confirm this hypothesis, although we also cannot discriminate between an outflow, a disk or other more complex kinematic structure. This will have to wait for higher angular resolution observations with e.g. ALMA.

4.5. Circumstellar Dust

4.5.1. W Hya

From the observed, unresolved, dust continuum of W Hya, we can determine whether stellar black body or thermal dust emission dominates the millimeter continuum. We estimate the stellar black body contribution using the following parameters for W Hya: distance, $D = 98$ pc (Vlemmings et al. 2003); stellar temperature, $T_{\text{eff}} = 2500$ K (Justtanont et al. 2005); and from this stellar radius, $R_{\text{star}} = 3.4 \times 10^{13}$ cm. Noting that T_{eff} and R_{star} vary significantly during the stellar pulsation cycle and have uncertainties of $\sim 25 - 50\%$ (e.g. Dehaes et al. 2007), so that this calculation is quite approximate, we estimate $S_{\text{star}, 1.4\text{mm}} = 158$ mJy. Thus, as was also found by Muller et al. (2008) at 1.1 mm, a significant component of the millimetre continuum is due to the star itself rather than dust. Using the Rayleigh-Jeans approximation to calculate dust mass, M_d , assuming optically thin emission, following Muller et al. (2007)

$$M_d = \frac{2c^2 D^2 a_d \rho_d (S_{\text{tot}} - S_{\text{star}})}{3Q_\nu k T_d \nu^2} \quad (3)$$

where grain size $a_d = 0.2 \mu\text{m}$, grain mass density $\rho_d = 3.5 \text{ g cm}^{-3}$ and emissivity $Q_\nu = 5.65 \times 10^{-4} (\nu/274.6 \text{ GHz})$, typical assumed values for oxygen-rich stars. Adopting a beam-averaged dust temperature $T_d = 700$ K, we obtain a dust mass $M_d = 4.9 \times 10^{-7} M_\odot$ within a radius of about 70 AU.

The millimeter dust observations do not probe averaged mass loss history over the entire circumstellar envelope, but instead can give a good indication of recent mass loss rate. For a W Hya expansion velocity of $V_{\text{exp}} = 7 \text{ km s}^{-1}$ (Dehaes et al. 2007), and a beam of ~ 1.5 arcseconds, we are probing material that has been ejected only over the past ≤ 50 years. We derive a gas+dust mass loss rate of $\geq 9.8 \times 10^{-7} M_\odot \text{ yr}^{-1}$, assuming a gas to dust ratio of 100. This is comparable to the distance-adjusted rate of $1.7 \times 10^{-6} M_\odot \text{ yr}^{-1}$ from ISO observations of Zubko & Elitzur (2000), and only slightly higher than the distance adjusted $4 \times 10^{-7} M_\odot \text{ yr}^{-1}$ value determined from ODIN observations by Justtanont et al. (2005).

4.5.2. VX Sgr

In order to estimate the central star black body contribution to the continuum of VX Sgr, we adopt $D = 1.57$ kpc (Chen et al. 2007), $R_{\text{star}} = 1.0 \times 10^{14}$ cm and $T_{\text{eff}} = 3200$ K (Monnier et al. 2004). At $\lambda = 1.4$ mm, we estimate that the stellar component is only $S_{\text{star}, 1.4\text{mm}} = 6.7$ mJy. Using Eqn. 3, the mass of the dust enclosed in a region of radius ~ 1300 AU is therefore $M_d = 2.1 \times 10^{-4} M_\odot$. Here we have also assumed a beam-averaged $T_d = 700$ K, based on results of Danchi et al. (1994). For the expansion velocity, Murakawa et al. (2003) find velocities of 10 and 20 km s^{-1} at the inner and outer edges of the water maser zone at 100 and 300 AU respectively. Adopting an average $V_{\text{exp}} = 15 \text{ km s}^{-1}$, the observed region corresponds to an age of about 400 years. We estimate a total gas+dust mass of $2.1 \times 10^{-2} M_\odot$ in this region, and therefore a recent mass-loss rate of $5.3 \times 10^{-5} M_\odot \text{ yr}^{-1}$. This is in reasonable agreement with other mass loss measurements e.g. $3.2 \times 10^{-5} M_\odot \text{ yr}^{-1}$ (Netzer 1989).

5. CONCLUSIONS

We have determined the magnetic field morphology at a few stellar radii from VX Sgr using SiO masers, and find that it is consistent with the interpretation in terms of a dipole magnetic field from OH and H₂O maser observations. This is the first evidence that circumstellar magnetic field morphology is conserved from close to the star to the outer edge of the CSE. As the magnetic field strengths measured in the OH and H₂O maser regions imply the magnetic field is dynamically important, a further extrapolation of this dipole field to the star ($\propto R^{-3}$) indicates that also in the SiO maser region the magnetic field dominates the kinetic and thermal energies, with an estimated field strength of $B \sim 25 - 100$ G.

Our images of the SiO masers around VX Sgr and W Hya show that the two $v = 1, 2$ rotational ^{28}SiO transitions as well as the ^{29}SiO $v = 0$ transition avoid each other. While a ring structure is seen in the ^{29}SiO line, the masers do not seem to be confined to a narrow region.

Finally, our SO $5_5 - 4_4$ observations reveal the possible presence of a slow bipolar outflow or a rotating, disk-like structure around W Hya. This structure is nearly perpendicular to the elliptically extended emission previously detected from the radio-photophere.

High angular resolution observations of submillimeter SiO masers and their polarization will become relatively straightforward with the Atacama Large Millime-

ter/submillimeter Array (ALMA). Extremely interesting science targets in their own right, the strength and high polarization fraction of the SiO masers also make them good ALMA polarization calibrators for a variety of frequency bands.

This research was supported by the Deutsche Forschungsgemeinschaft (DFG) through the Emmy Noether Research grant VL 61/3-1.

REFERENCES

- Barvainis, R., McIntosh, G., & Predmore, C. R. 1987, *Nature*, 329, 613
- Cernicharo, J., Bujarrabal, V., & Santaren, J. L. 1993, *ApJ*, 407, L33
- Chapman, J. M., & Cohen, R. J. 1986, *MNRAS*, 220, 513
- Chen, X., Shen, Z.-Q., Imai, H., & Kamohara, R. 2006, *ApJ*, 640, 982
- Chen, X., Shen, Z.-Q., & Xu, Y. 2007, *Chinese J. Astron. Astrophys.*, 7, 531
- Chen, X., & Shen, Z.-Q. 2008, *ApJ*, 681, 1574
- Cotton, W. D., et al. 2004, *A&A*, 414, 275
- Cotton, W. D., Perrin, G., & Lopez, B. 2008, *A&A*, 477, 853
- Danchi, W. C., Bester, M., Degiacomi, C. G., Greenhill, L. J., & Townes, C. H. 1994, *AJ*, 107, 1469
- Dehaes, S., Groenewegen, M. A. T., Decin, L., Hony, S., Raskin, G., & Blommaert, J. A. D. L. 2007, *MNRAS*, 377, 931
- Dinh-V.-Trung, Muller, S., Lim, J., Kwok, S., & Muthu, C. 2009, *ApJ*, 697, 409
- Efron, B., & Tibshirani, R. 1991, *Science*, 253, 390
- Goldreich, P., Keeley, D. A., & Kwan, J. Y. 1973, *ApJ*, 179, 111
- Gomez Balboa, A. M., & Lepine, J. R. D. 1986, *A&A*, 159, 166
- Gray, M. D., Humphreys, E. M. L., & Yates, J. A. 1999, *MNRAS*, 304, 906
- Greenhill, L. J., Colomer, F., Moran, J. M., Backer, D. C., Danchi, W. C., & Bester, M. 1995, *ApJ*, 449, 365
- Herpin, F., & Baudry, A. 2000, *A&A*, 359, 1117
- Herpin, F., Baudry, A., Thum, C., Morris, D., & Wiesemeyer, H. 2006, *A&A*, 450, 667
- Ho, P. T. P., Moran, J. M., & Lo, K. Y. 2004, *ApJ*, 616, L1
- Humphreys, E. M. L., Gray, M. D., Yates, J. A., & Field, D. 1997, *MNRAS*, 287, 663
- Humphreys, E. M. L. 1999, Ph.D. Thesis, Bristol University, UK
- Jewell, P. R., Dickinson, D. F., Snyder, L. E., & Clemens, D. P. 1987, *ApJ*, 323, 749
- Justtanont, K., et al. 2005, *A&A*, 439, 627
- Kemball, A. J., & Diamond, P. J. 1997, *ApJ*, 481, L111
- Kemball, A., & Martinsek, A. 2005, *AJ*, 129, 1760
- Kemball, A. J. 2007, *IAU Symposium*, 242, 236
- Kemball, A., Martinsek, A., Mitra, M., & Chiang, H.-F. 2010, *AJ*, 139, 252
- Lockett, P., & Elitzur, M. 1992, *ApJ*, 399, 704
- Monnier, J. D., et al. 2004, *ApJ*, 605, 436
- Muller, S., Dinh-V.-Trung, Lim, J., Hirano, N., Muthu, C., & Kwok, S. 2007, *ApJ*, 656, 1109
- Muller, S., Dinh-V.-Trung, He, J.-H., & Lim, J. 2008, *ApJ*, 684, L33
- Murakawa, K., Yates, J. A., Richards, A. M. S., & Cohen, R. J. 2003, *MNRAS*, 344, 1
- Nedoluha, G. E., & Watson, W. D. 1990, *ApJ*, 361, L53
- Nedoluha, G. E., & Watson, W. D. 1994, *ApJ*, 423, 394
- Netzer, N. 1989, *ApJ*, 342, 1068
- Omont, A., Lucas, R., Morris, M., & Guilloteau, S. 1993, *A&A*, 267, 490
- Pardo, J. R., Cernicharo, J., Gonzalez-Alfonso, E., & Bujarrabal, V. 1998, *A&A*, 329, 219
- Reid, M. J., & Menten, K. M. 2007, *ApJ*, 671, 2068
- Reid, M. J., & Moran, J. M. 1988, *Galactic and Extragalactic Radio Astronomy*, 255
- Sánchez Contreras, C., Bujarrabal, V., Neri, R., & Alcolea, J. 2000, *A&A*, 357, 651
- Soria-Ruiz, R., Alcolea, J., Colomer, F., Bujarrabal, V., Desmurs, J.-F., Marvel, K. B., & Diamond, P. J. 2004, *A&A*, 426, 131
- Shinnaga, H., Moran, J. M., Young, K. H., & Ho, P. T. P. 2004, *ApJ*, 616, L47 (S04)
- Soria-Ruiz, R., Colomer, F., Alcolea, J., Bujarrabal, V., Desmurs, J.-F., & Marvel, K. B. 2005, *A&A*, 432, L39
- Szymczak, M., & Cohen, R. J. 1997, *MNRAS*, 288, 945
- Szymczak, M., Cohen, R. J., & Richards, A. M. S. 1998, *MNRAS*, 297, 1151
- Szymczak, M., Cohen, R. J., & Richards, A. M. S. 2001, *A&A*, 371, 1012
- van der Veen, W. E. C. J., Omont, A., Habing, H. J., & Matthews, H. E. 1995, *A&A*, 295, 445
- Vlemmings, W. H. T., van Langevelde, H. J., Diamond, P. J., Habing, H. J., & Schilizzi, R. T. 2003, *A&A*, 407, 213
- Vlemmings, W. H. T., van Langevelde, H. J., & Diamond, P. J. 2005, *A&A*, 434, 1029
- Vlemmings, W. H. T. 2007, *IAU Symposium*, 242, 37
- Western, L. R., & Watson, W. D. 1984, *ApJ*, 285, 158
- Wishnow, E. H., Townes, C. H., Walp, B., & Lockwood, S. 2010, *ApJ*, 712, L135
- Zubko, V., & Elitzur, M. 2000, *ApJ*, 544, L137